Inorg. Chem. **2005**, *44*, 8503–8509

One-Dimensional $BiPO_4$ Nanorods and Two-Dimensional BiOCl Lamellae: Fast Low-Temperature Sonochemical Synthesis,Characterization, and Growth Mechanism

Jun Geng,[†,§] Wen-Hua Hou,[†] Yi-Nong Lv,[‡] Jun-Jie Zhu,*[,†] and Hong-Yuan Chen[†]

Department of Chemistry, Key Laboratory of Analytical Chemistry for Life Science, Nanjing University, Nanjing 210093, P. R. China, and College of Materials Science and Engineering, Nanjing University of Technology, Nanjing 210009, P. R. China

Received May 2, 2005

Regular $BiPO_4$ nanorods, for the first time, and BiOCl lamellae have been successfully synthesized via a facile sonochemical method in a surfactant/ligand-free system under ambient air. The as-prepared products are characterized by XRD, TEM, SAED, FE-SEM, HRTEM, and Raman spectroscopy. The effects of pH and ultrasound irradiation on the phase and morphology of the products are studied and the sonochemical formation mechanisms of 1D and 2D structures are discussed. TEM data from samples made after different reaction times suggest an ultrasound-induced nucleation and an oriented-attachment growth mechanism.

Introduction

Besides the conventional 1D nanorods, nanowires, and nanotubes,[1−3] plenty of new 2D nanomaterials, such as nanodisks, nanosheets, and nanofilms, have emerged recently.[4−6] Such accomplishments confirm the tremendous worldwide efforts to create advanced and functional building blocks for the development of innovative nanomaterials and smart nanodevices. The design of well-defined and highly oriented nanomaterials and their large-scale manufacturing at low cost, in particular, remain crucial challenges to unfold the very promising future of nanotechnology.

Bismuth and its compounds have been widely studied recently because of their unique qualities.[7,8] Among them, bismuth phosphates ($BiPO_4$) were reported to be good catalysts,[9,10] orthophosphate ion-sensors,[11] and could be used as a separating agent for uranium, neptunium, and americium.[12−14] $BiPO_4$ is also considerably important for improving the electrical properties of phosphate glasses, which are of technological interest as ionic, electronic, and fast ionic conductors.[15,16] However, to the best of our knowledge, there is no report on the preparation of nanostructured $BiPO_4$, so far. $Bi^{III}-VI^{A}-VII^{A}$ compounds such as BiOCl, BiSCl, and BiSI evoked great interest because of the coexistence of several physical properties.[17,18] For example, BiOCl shows the properties of photoluminescence, thermally stimulated conductivity, and good catalytic activity and selectivity in the oxidative coupling of the methane (OCM) reaction.[19,20]

* To whom correspondence should be addressed. E-mail: jjzhu@nju.edu.cn. Phone and Fax: +86-25-83594976.

† Department of Chemistry, Key Laboratory of Analytical Chemistry for Life Science.

‡ College of Materials Science and Engineering.

§ Permanent address: Department of Chemistry, Jiangsu Institute of Education, Nanjing, 210013, P. R. China.

(1) Vayssieres, L. *Encyclopedia of Nanoscience and Nanotechnology;* American Scientific Publishers: Stevenson Ranch, CA, 2004; Vol. 8, pp 147−166.
(2) Dai, Z. R.; Pan, Z. W.; Wang, Z. L. *Adv. Funct. Mater.* **2003**, *13*, 9.
(3) Patzke, G. R.; Krumeich, F. K.; Nesper, R. *Angew. Chem., Int. Ed.* **2002**, *41*, 2446.
(4) Schmidt, O. G.; Eberl, K. *Nature* **2001**, *410*, 168.
(5) Ma, R. Z.; Bando, Y.; Sasaki, T. *J. Phys. Chem. B* **2004**, *108*, 2115.
(6) Li, F.; Ding, Y.; Gao, P. X.; Xin, X. Q.; Wang, Z. L. *Angew. Chem., Int. Ed.* **2004**, *43*, 5238.
(7) Molares, M.; Chtanko, N.; Cornelius, T. W.; Dobrev, D.; Enculescu, I.; Blick, R. H.; Neumann, R. *Nanotechnology* **2004**, *15*, 201.
(8) Koh, Y. W.; Lai, C. S.; Du, A. Y.; Tiekink, E.; Loh, K. P. *Chem. Mater.* **2003**, *15*, 4544.
(9) Chang, T. S.; Li, G. J.; Shin, C. H.; Lee, Y. K.; Yun, S. S. *Catal. Lett.* **2000**, *68*, 229.
(10) Takita, Y.; Ninomiya, M.; Miyake, H.; Wakamatsu, H.; Yoshinaga, Y. *Phys. Chem. Chem. Phys.* **1999**, *1*, 4501.
(11) Iitaka, K.; Tani, Y.; Umezawa, Y. *Anal. Chim. Acta* **1997**, *338*, 77.
(12) Kalaiselvan, S.; Jeevanram, R. K. *J. Radioanal. Nucl. Chem.* **1999**, *240*, 277.
(13) Holgye, Z. *J. Radioanal. Nucl. Chem.* **1998**, *227*, 127.
(14) Charyulu, M. M.; Chetty, K. V.; Phal, D. G.; Sagar, V.; Naronha, D. M.; Pawar, S. M.; Swarup, R.; Ramakrishna, V. V.; Venugopal, V. *J. Radioanal. Nucl. Chem.* **2002**, *251*, 153.
(15) Elmoudane, M.; Et-tabirou, M.; Hafid, M. *Mater. Res. Bull.* **2000**, *35*, 279.
(16) Jermoumi, T.; Hafid, M.; Et-tabirou, M.; Taibi, M.; ElQadim, H.; Toreis, N. *Mater. Sci. Eng. B* **2001**, *85*, 28.
(17) Berlincourt, D. *J. Acoust. Soc. Am.* **1992**, *91*, 3034.
(18) Whatmore, R. W. *Rep. Prog. Phys.* **1996**, *49*, 1335.

10.1021/ic050674g CCC: $30.25
Published on Web 10/20/2005

Several efforts have been made to prepare such multielemental inorganic materials,[21−23] and it is still a challenge to prepare the material by a fast and convenient method.

In recent years, sonochemical techniques have been extensively used in the synthesis of nanostructured materials.[24−26] During the acoustic cavitation process, very high temperatures (>5000 K), pressures (>20 MPa), and cooling rates (>10^{10} K/s) can be achieved upon the collapse of the bubble.[27] Such remarkable environments provide a unique platform for the growth of novel nanostructures. In this paper, we present a facile procedure for the one-step selective synthesis of 1D $BiPO_4$ nanorods and 2D BiOCl lamellae via a sonochemical method. We found that ultrasonic irradiation and the pH value of the reaction system played important roles in the formation of the final nanomaterials.

Experimental Section

All the reagents used were of analytical purity and used without further purification. $Bi(NO_3)_3{\cdot}5H_2O$ was purchased from Beijing Chemical Reagents Factory of China. $Na_3PO_4{\cdot}12H_2O$, concentrated HCl, and HNO_3 were purchased from Shanghai Chemical Reagent Limited Corporation of China. In a typical preparation of $BiPO_4$ nanorods, 20 mM $Bi(NO_3)_3{\cdot}5H_2O$ and 20 mM $Na_3PO_4{\cdot}12H_2O$ were mixed, and the pH value of the mixture was adjusted with 4 M HNO_3 to the range of 0.5−1. The solution was exposed to high-intensity ultrasonic irradiation under ambient air. Ultrasonic irradiation was accomplished with a high-intensity ultrasonic probe (Xinzhi Co., China, JY92−2D, 0.6 cm diameter; Ti-horn, 20 kHz, 60W/cm^2) immersed directly in the reaction solution. The total reaction time was 30 min. The sonication was conducted without cooling so that a temperature of about 333 K was reached at the end of the reaction. A white precipitate was centrifuged, after the reactant was cooled to room temperature; then it was washed with distilled water and absolute ethanol in sequence and dried in air. In the selective preparation of layered BiOCl nanocrystals, all the procedures remained the same as above except that the pH value of the solution was adjusted with 6 M HCl instead of 4 M HNO_3. The final products were characterized by XRD, SEM, TEM, SAED, HRTEM, and Raman spectroscopy.

The XRD (X-ray diffraction) analysis was performed by a Philips X-pert X-ray diffractometer at a scanning rate of 4° min^{-1} in the 2θ range from 10° to 80°, with graphite monochromatized Cu Kα radiation ($\lambda = 0.15418$ nm). Scanning electron micrographs (SEM) and energy-dispersive X-ray analysis (EDAX) patterns were taken on a LEO-1530VP field-emission scanning electron microscope. Transmission electron micrographs (TEM) and selected area electron diffraction (SAED) patterns were recorded on a JEOLJEM 200CX transmission electron microscope, using an accelerating voltage of 200 kV. High-resolution transmission electron micrographs (HRTEM) were obtained by employing a JEOL-2010 high-resolution transmission electron microscope with a 200 kV accelerating voltage. The Raman spectra were recorded on a JY HR-800 spectrometer provided by JY Company at room temperature with an excitation wavelength of 488 nm.

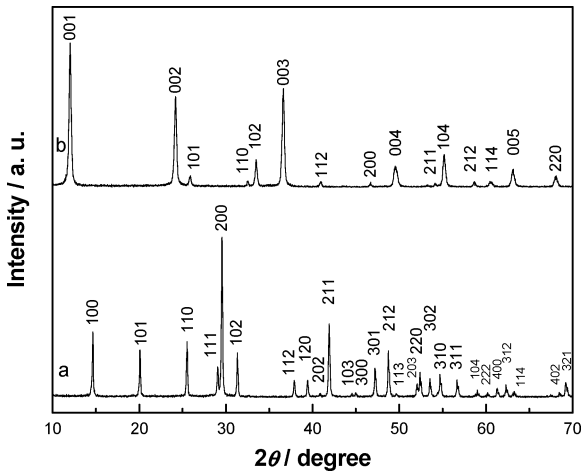

Figure 1. The XRD patterns of the as-prepared products: (a) $BiPO_4$ and (b) BiOCl.

Results and Discussion

Characterizations of $BiPO_4$ and BiOCl. The XRD pattern of the as-prepared $BiPO_4$ (Figure 1a) could be indexed to the hexagonal primitive cell (JCPDS Cards 45-1370) with lattice constants of $a = 6.978$ Å and $c = 6.474$ Å. The (200) peak appeared to have a quite strong intensity, indicating that the crystalline $BiPO_4$ was oriented in a particular crystallographic direction. The XRD pattern of single-crystal BiOCl (Figure 1b) could be indexed in terms of tetragonal symmetry with a space group of *P*4/*nmm* and lattice constants of $a = 3.888$ Å and $c = 7.357$ Å. In contrast to that of the bulk BiOCl (JCPDS Cards 82-0485), the five peaks (001), (002), (003), (004), and (005) at 2θ of 12.04°, 24.20°, 36.64°, 49.54°, and 63.16°, respectively, showed extraordinarily strong intensity, which indicated single crystals in the form of platelets with the *c* axis perpendicular to the platelets.

A typical SEM image of $BiPO_4$, shown in Figure 2a, reveals that this sample is composed of nanorods with diameters of 40−60 nm and lengths of 2−5μm, which shows a large aspect ratio of 50−80. The high-magnification SEM image exhibits the faceted morphology of $BiPO_4$ nanorods (Figure 2b) and the six-faceted trunk can be identified. The SAED pattern (inset of Figure 2c) recorded on an individual $BiPO_4$ nanorod reveals the single-crystalline nature of the sample with a preferential growth oriented along the (001) crystalline plane. The HRTEM image (Figure 2d) shows that the sample is structurally uniform with an interplanar spacing of about 0.35 nm, which corresponds to the (110) lattice spacing of hexagonal $BiPO_4$. Combined with SAED observations, we are able to draw the conclusion that these $BiPO_4$ nanorods preferentially grow along the [001] direction.

The BiOCl crystals display a lamellar structure composed of square nanosheets (Figure 3a and c) with dimensions of (1−4) × (1−4) μm^2. Careful observation shows that the sheetlike crystals grow layer by layer, and the sheet thickness

(19) Shtilikha, M. V.; Chepur, D. V. *Sov. Phys.−Semicond.* **1972**, *16*, 962.
(20) Kijima, N.; Matano, K.; Saito, M.; Oikawa, T.; Konishi, T.; Yasuda, H.; Sato, T.; Yoshimura, Y. *Appl. Catal. A* **2001**, *206*, 237.
(21) Ganesha, R.; Arivuoli, D.; Ramasamy, P. *J. Cryst. Growth* **1993**, *128*, 1081.
(22) Dellinger, T. M.; Braun, P. V. *Scr. Mater.* **2001**, *44*, 1893.
(23) Zhu, L. Y.; Xie, Y.; Zheng, X. W.; Yin, X.; Tian, X. B. *Inorg. Chem.* **2002**, *41*, 4560.
(24) Mdleleni, M. M.; Hyeon, T.; Suslick, K. S. *J. Am. Chem. Soc.* **1998**, *120*, 6189.
(25) Gedanken, A. *Ultrason. Sonochem.* **2004**, *11*, 47.
(26) Okitsu, K.; Yue, A.; Tanabe, S.; Matsumoto, H.; Yobiko, Y.; Yoo, Y. B. *Chem. Soc. Jpn.* **2002**, *75*, 2289.
(27) Suslick, K. S.; Choe, S. B.; Cichowlas, A. A.; Grinstaff, M. W. *Nature* **1991**, *353*, 414.

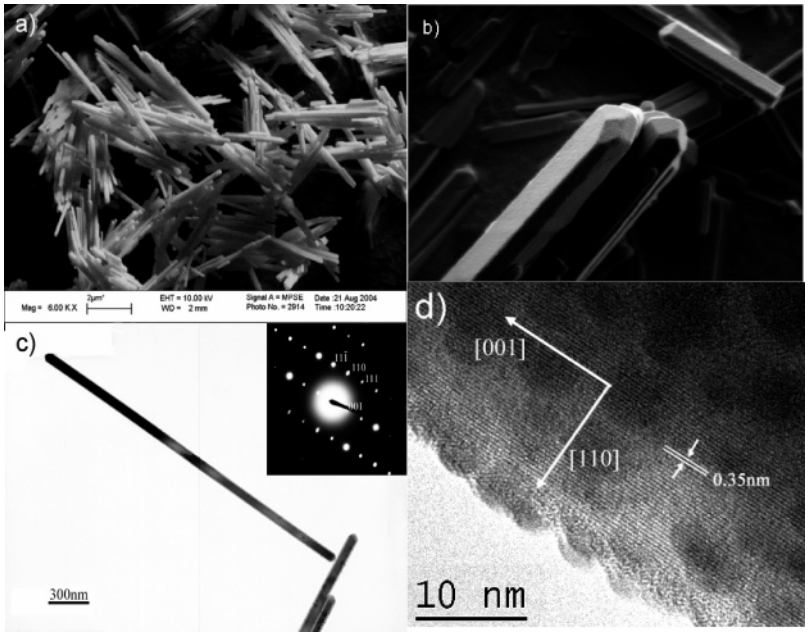

Figure 2. (a) Low-magnification and (b) high-magnification SEM images of $BiPO_4$ nanorods, (c) a typical TEM image and SAED pattern recorded on a single $BiPO_4$ nanorod, and (d) a HRTEM image of the $BiPO_4$ nanorod.

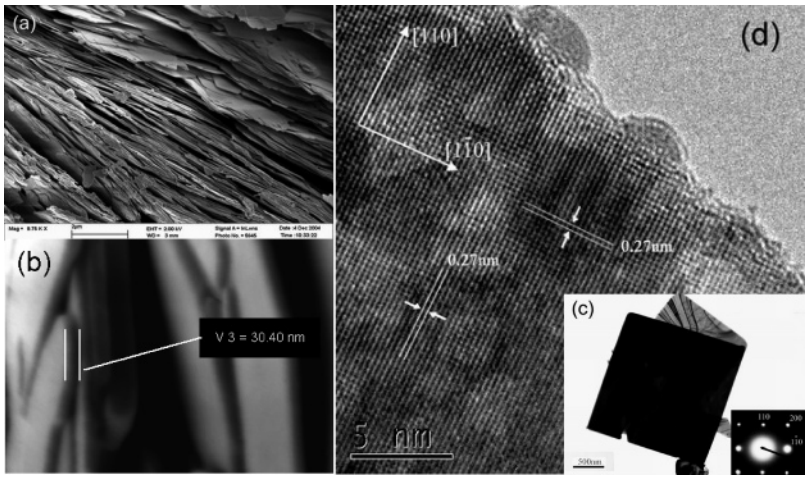

Figure 3. (a) Low-magnification SEM image of BiOCl lamellae, (b) a high-magnification SEM image showing the thickness of the lamella to be about 30 nm, (c) a typical TEM image and SAED pattern of a single BiOCl nanosheet, and (d) a HRTEM image of the BiOCl lamella.

is in the range of 20−30 nm (Figure 3b). The SAED pattern of BiOCl (inset of Figure 3c) indicates that the layered structure is perpendicular to the *c* axis. The HRTEM image of a single BiOCl nanosheet (Figure 3d) exhibits good crystalline and clear lattice fringes. The interplanar spacing is 0.27 nm corresponding to the {110} planes of the tetragonal system of BiOCl. The HRTEM observation confirms, along with the XRD and SAED results, that these BiOCl lamellae are perpendicular to the *c* axis.

To further characterize the single-crystalline $BiPO_4$ and BiOCl, the Raman spectra are presented for $BiPO_4$ in the 100−1400 cm^{-1} region and BiOCl in the range of 100−1000 cm^{-1}. As far as we know, the Raman spectrum of $BiPO_4$ has rarely been investigated. The experimental frequency values of the free PO_4^{3-} modes commonly quoted in the literature[28−30] were obtained by Raman measurements dating back to the 1930s. In the Raman spectrum of $BiPO_4$ (Figure 4), the intense band observed at 963 cm^{-1} is assigned to the ν_1 PO_4 symmetric stretching mode. The Raman band at 1060 cm^{-1} is ascribed to the ν_3 PO_4 antisymmetric stretching mode. The Raman spectrum also displays bands at 591, 560, and 474 cm^{-1}, which correspond to the ν_4 bending modes of the PO_4 units. Two bands are observed at 446 and 398 cm^{-1} and are considered to have originated from the ν_2 bending modes of the PO_4 units. The Raman spectrum displays an intense band at 201 cm^{-1}, which may be assigned to an OBiO symmetric bending mode. One of the strong features of Raman spectroscopy is that bands below 400 cm^{-1} are readily determined. This means that intense bands attributable to M−O vibrations can be ascertained.[31]

(28) Kravitz, L. C.; Kingsley, J. D.; Elkin, E. L. *J. Chem. Phys.* **1968**, *49*, 4600.

(29) Boyer, L. L.; Fleury, P. A. *Phys. Rev. B* **1974**, *9*, 2693.

(30) Herzberg, G. *Molecular Spectra and Molecular Structure II. Infra-Red and Raman Spectra of Polyatomic Molecules*; D. Van Nostrand: Princeton, NJ, 1945.

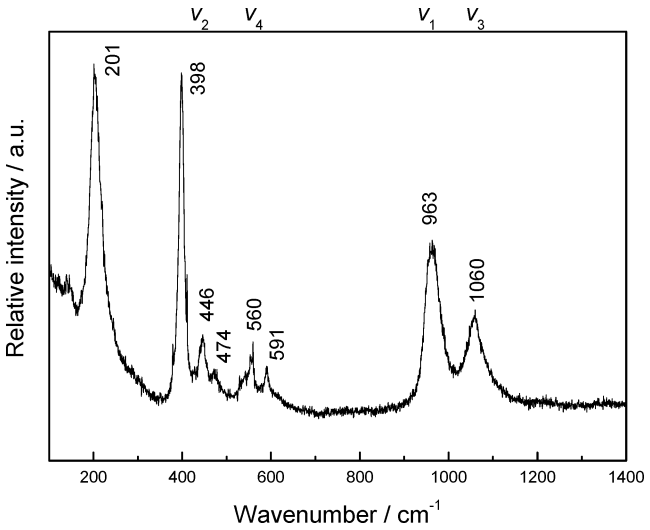

Figure 4. The Raman spectrum of $BiPO_4$. The normal-mode frequencies of the free PO_4^{3-} ion are indicated on the top frequency axis by ν_1, ν_2, ν_3, and ν_4.

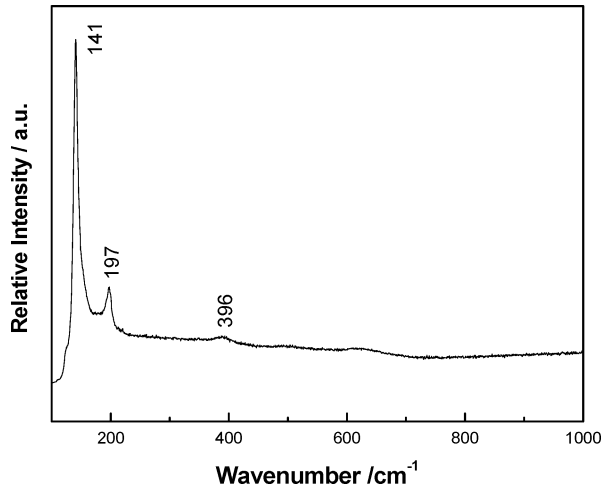

Figure 5. The Raman spectrum of lamellar BiOCl.

Isostructural BiOCl is a tetragonal PbFCl-type structure with space group *P*4/*nnm*. For such a structure of space group D_{4h}^7, with two molecular formulas per unit cell, the Raman active modes are two A_{1g}, B_{1g}, and E_g. Figure 5 consists of two distinguished bands and one weak band. Because symmetric vibrations often give rise to more intense Raman bands than asymmetric vibrations, the strong band at 141 cm^{-1} is assigned to the A_{1g} internal Bi−Cl stretching mode. The band at 197 cm^{-1} can be assigned to the E_g internal Bi−Cl stretching mode, while the E_g external Bi−X stretching is probably masked by the strong band at 141 cm^{-1}. The E_g and B_{1g} band, produced by motion of the oxygen atoms, at about 396 cm^{-1} is very weak and is not easy to observe. The wavenumber here is similar to the reported values in ref 23 but slightly smaller than that in the reference measure of powder BiOCl,[32] which probably derives from the stronger orientation of lamellar single crystals than that of powders.

Effect of pH Value. The pH value played a key role in the synthesis of 1D $BiPO_4$ and 2D BiOCl nanocrystals. The uniform $BiPO_4$ nanorods with a large aspect ratio could only be obtained when the reaction system was adjusted by HNO_3 to the pH range of 0.5−1. With the increase of pH value, the tendency to grow along a certain direction had been weakened to some extent, and the $BiPO_4$ prepared had lower aspect ratios and less-uniform morphologies (Figure 6 and Table 1). On the other hand, when the pH value was lower than 0.5, no products were obtained because the white precipitate could be dissolved in such acidic solution. According to Peng et al.,[33] the high chemical potential generated by a high monomer concentration in the growth solution favors the growth of 1D nanocrystals. Meanwhile, faster ionic motion usually ensures a reversible pathway between the fluid phase and the solid phase, which allows atoms, ions, or molecules to adopt correct positions in developing crystal lattices.[34] In the present case, the main reaction may take place as follows

$$Bi^{3+} + H_nPO_4^{(3-n)-} = BiPO_4\downarrow + nH^+ \qquad (1)$$

The strong pH-dependent relationship with the morphologies of the products is the result of the sensitive influence of the pH on the solute concentrations ([Bi^{3+}] and [$H_nPO_4^{(3-n)-}$]). When the pH value of the solution before sonication was alkaline, nucleation occurred at an outburst speed forming a large quantity of $BiPO_4$ precipitation, which led to low Bi^{3+} and $H_nPO_4^{(3-n)-}$ concentrations, low chemical potential, and slow ion motion. As the pH value of the solution was lowered by HNO_3, the white precipitate was gradually dissolved resulting in higher solute concentrations. When the pH value

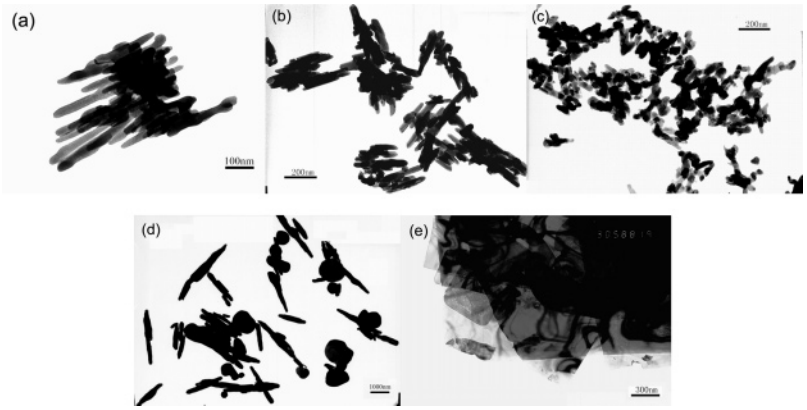

Figure 6. TEM images of as-prepared products under various pH conditions: (a) adjusted by HNO_3 to pH 2, (b) pH 4, and (c) pH 7 and adjusted by HCl to (d) pH > 1 and (e) pH 0.5−1.

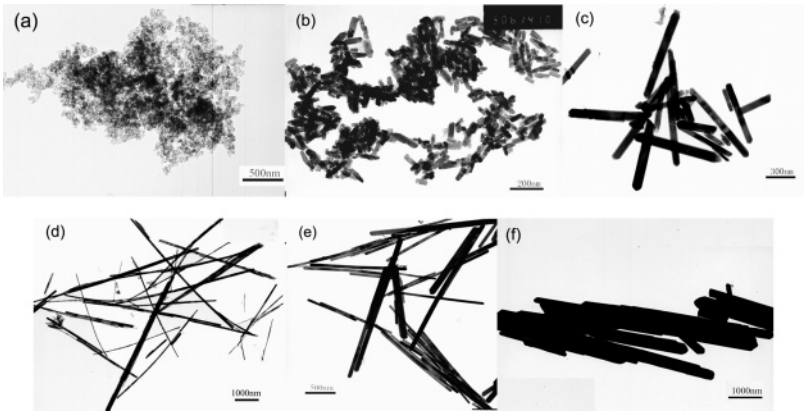

Figure 7. TEM images of $BiPO_4$ obtained after sonication for (a) 2, (b) 5, (c) 8, (d) 15, (e) 25, and (f) 60 min. A growth process from primary particles to short nanorods then to longer nanorods is clearly observed.

Table 1. Influence of pH on the Crystal Structures and Morphologies of the Products

acid	pH	precipitation	XRD	morphology	size
HNO_3	0.5−1	gradual	$BiPO_4$	uniform nanorods	(40−60) nm × (2−5) μm
	2	instant	$BiPO_4$	less uniform nanorods	(20−40) nm × (150−500) nm
	4	instant	$BiPO_4$	unhomogeneous nanorods	(30−40) nm × (100−250)nm
	no adjustment	instant	$BiPO_4$	aggregated and irregular rodlike nanoparticles	(20−30) nm × (50−150) nm
HCl	≤1	gradual	BiOCl	lamellae	(1−4) × (1−4) μm^2
	>1	instant	$BiPO_4$ + BiOCl	nanorods + nanosheets	−

decreased to the range of 0.5−1, the precipitate was completely dissolved to form a clear solution. So the solute concentrations, the chemical potential, and the rate of the ion motion arrived at the maximum value, which ensured the 1D anisotropic growth. Considering the above factors, hexagonal $BiPO_4$ nanorods can be grown in an acid environment, especially in the pH range of 0.5−1.

When HCl solution was used to adjust the pH value instead of HNO_3, the final product was not $BiPO_4$ but BiOCl. Because the solubility product constant (K_{sp}) of BiOCl (1.8×10^{-31}, 298.15 K) is much smaller than that of $BiPO_4$ (1.3×10^{-23}, 298.15 K) and when there was a large quantity of Cl^- anion in the solution, the final product was lamellar BiOCl, as the result of competitive reaction between eq 1 and eq 2.

$$Bi^{3+} + H_2O + Cl^- = BiOCl\downarrow + 2H^+ \qquad (2)$$

Therefore, $BiPO_4$ nanorods or BiOCl lamellae could be selectively synthesized simply through choosing the pH regulator and controlling the pH value. We have also done a comparative experiment keeping other preparation conditions unchanged but without the addition of Na_3PO_4. In this case, only the irregularly shaped BiOCl was obtained, which infers that the PO_4^{3-} ion may play a role in the formation of lamellar structure.

Effect of Ultrasonic Irradiation and Possible Formation Mechanism. High-intensity ultrasonic irradiation also played an important role in the formation of 1D and 2D products. The transient high-temperature and high-pressure field produced during ultrasonic irradiation provides a favorable environment for the anisotropic growth of the nanocrystals. Without sonication, $BiPO_4$ and BiOCl were hardly acquired and the morphology was irregular. To investigate the details of the sonochemical conversion from precursor to final products, we have carried out a series of experiments by employing different sonication times without changing other preparation conditions.

In the case of $BiPO_4$, after the solution was exposed to sonication for 2 min, the clear solution became turbid (Figure 7a). EDAX measurements revealed that this precipitate was pure $BiPO_4$. No diffraction peak was detected in the XRD pattern of this sample, indicating that the $BiPO_4$ powders obtained after 2 min of sonication was amorphous. It has been known that three different regions are formed during the aqueous sonochemical process:[35] (1) the inner environment (gas phase) of the collapsing bubble, where elevated temperatures (several thousands of degrees) and pressures (hundreds of atmospheres) are produced; (2) the interfacial region between the cavitation bubbles and the bulk solution, where the temperature is lower than in the gas-phase region but still high enough to rupture chemical bonds and induce a variety of reactions; and (3) the bulk solution, which is at ambient temperature and where the reaction between reactant molecules and radicals takes place. It is generally observed that if the reaction occurs inside the collapsing bubbles, the product obtained is amorphous because of the very high quenching rate experienced by the products. On the other hand, if the reaction takes place in the interfacial or bulk regions, one would expect to get crystalline products.[36] In

(31) Frost, R. L.; Weier, M. L.; Erickson, K. L.; Carmody, O.; Mills, S. J. *J. Raman Spectrosc.* **2004**, *35*, 1047.
(32) Davies, J. E. D. *J. Inorg. Nucl. Chem.* **1973**, *35*, 1531.
(33) Peng, Z. A.; Peng, X. G. *J. Am. Chem. Soc.* **2001**, *123*, 1389.
(34) Trentler, T. J.; Hickman, K. M.; Goel, S. C.; Viano, A. M.; Gibbons, P. C.; Buhro, W. E. *Science* **1995**, *270*, 1791.
(35) (a) McNamara, W. B.; Didenko, Y. T.; Suslick, K. S. *Nature* **1999**, *401*, 772. (b) Suslick, K. S.; Hammerton, D. A.; Cline, R. E. *J. Am. Chem. Soc.* **1986**, *108*, 5641. (c) Grinstaff, M. W.; Cichowlas, A. A.; Choe, S. B.; Suslick, K. S. *Ultrasonics* **1992**, *30*, 168.
(36) Jeevanandam, P.; Koltypin, Y.; Gedanken, A.; Mastai, Y. *J. Mater. Chem.* **2000**, *10*, 511.

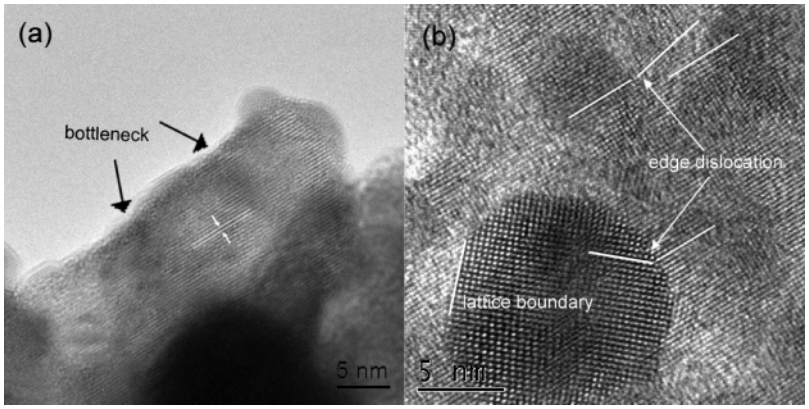

Figure 8. HRTEM images of aggregated particles at the early stage of crystal growth of (a) $BiPO_4$ and (b) BiOCl. Panel a shows that the clear parallel crystallographic orientation and the bottlenecks between the fused adjacent particles are still visible. White arrows in panel b highlight the boundaries in which there are some dislocations between primary particles. We assume that the primary particles may have aggregated in an oriented fashion, producing assemblies of oriented nanoparticles that subsequently underwent further growth (in the case of a) or they may have aggregated in a random manner and undergone recrystallization to result in parallel orientation of the primary particles (in the case of b).

the present case, because of the nonvolatile nature of Bi^{3+}, only a negligible amount of Bi^{3+} ion is expected to be present inside the cavity or bubble for a sonochemical reaction. However, amorphous $BiPO_4$ nanoparticles were obtained at the early stage of the reaction, implying that the nuclei formation of this sample probably occurs inside the collapsing bubbles. This contradictory phenomenon makes it quite difficult to explain the detailed nucleation mechanism at this moment and further work is still under way.

After an ultrasonic treatment of 5 min, a large quantity of white precipitate began to form. A typical TEM image (Figure 7b) reveals that the sample was composed of uniform nanorods with diameters of 20−30 nm and lengths of 50−100 nm. The XRD results proved that this precipitate was a crystalline hexagonal structure. When the reaction time increased to 8 min, the rods grew to diameters of 40−60 nm and lengths up to 1 μm (Figure 7c). After 15 min of sonication, the diameters of the nanorods were invariable, but the lengths increased to 2−5 μm (Figure 7d). During these stages, we assume that the ultrasonic irradiation further accomplished the crystallization of the amorphous $BiPO_4$ and the preferential 1D growth of nanocrystals. Cavitations and shock waves created by ultrasound can accelerate solid particles to high velocities leading to interparticle collisions and inducing an effective melting at the point of collision.[37] The energy generated during collision can induce the crystallization of the amorphous particles. The improvement of mass transport from turbulent mixing induced by cavitations also contributed to the uniform morphologies of the final products.[38] Detailed HRTEM images of a series of aggregated particles at the early stage of the crystal growth indicate an oriented-attachment growth. In this process, primary particles may aggregate in an oriented fashion to produce a larger single crystal, or they may aggregate randomly and reorient, recrystallize, or undergo phase transformations to produce larger single crystals. This kind of growth mode could lead to the formation of faceted particles or anisotropic growth if there is a sufficient difference in the surface energies of different crystallographic faces.[39] The $BiPO_4$ prepared here possessed a hexagonal crystal structure, which exhibited anisotropic growth preferentially along the [001] direction. It is well-known that the hexagonal crystal structure, such as ZnO and CdSe, often shows the anisotropic growth along the [001] direction.[33,40] Therefore, the anisotropic growth is believed to be the inherent driving force in the process of growing the hexagonal nanorods.[41]

This aggregation-growth mechanism provides a route for the incorporation of defects, such as edge and screw dislocations, in stress-free and initially defect-free nanocrsytalline materials.[42] In the HRTEM images (Figure 8), the vast majority of particles appear to be composed of many primary building-block particles ranging in size from less than 5 nm to 10 nm. It is seen that the lattice planes of the depicted particles are almost perfectly aligned and the lattice planes go straight through the contact areas. The bottlenecks between the two fused adjacent particles are still visible (Figure 8a). Some edge dislocations at the interface between the two primary building-block particles could be clearly detected (Figure 8b). We assume that the primary particles may have aggregated in an oriented fashion, producing assemblies of oriented nanoparticles that subsequently underwent further growth (in the case of Figure 8a), or they may have aggregated in a random manner, undergone recrystallization to result in a parallel orientation (in the case of Figure 8b).

Therefore, the sonochemical formation of $BiPO_4$ nanorods can be divided into three steps in sequence: (1) ultrasound-induced nuclei formation which leads to amorphous primary $BiPO_4$ nanopaticles, (2) ultrasound-induced oriented self-assembly of these primary nanoparticles to form the chain-type structure of $BiPO_4$ and generation of nanocrystalline short rods, and (3) a crystal growth process, resulting in the

(37) Doktycz, S. J.; Suslick, K. S. *Science* **1990**, *247*, 1067.
(38) Suslick, K. S.; Price, G. J. *Annu. Rev. Mater. Sci.* **1999**, *29*, 295 and the references therein.
(39) Penn, R. L.; Oskam, G.; Strathmann, T. J.; Searson, P. C.; Stone, A. T.; Veblen, D. R. *J. Phys. Chem. B* **2001**, *105*, 2177.
(40) Vayssieres, L. *Adv. Mater.* **2003**, *15*, 464.
(41) Wang, X.; Li, Y. D. *Angew. Chem., Int. Ed.* **2002**, *41*, 4790.
(42) Penn, R. L.; Banfield, J. F. *Science* **1998**, *281*, 969.

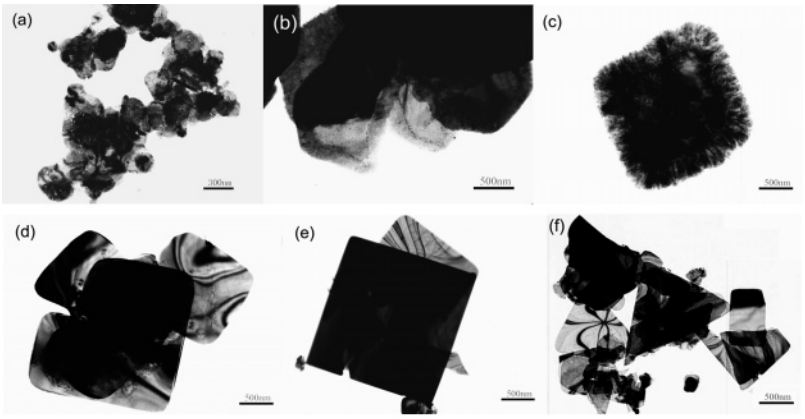

Figure 9. TEM images of BiOCl obtained after sonication for (a) 2, (b) 5, (c) 8, (d) 15, (e) 25, and (f) 60 min. The coarse fringes of lamellae became smooth, which indicates an aggregation and crystallization process.

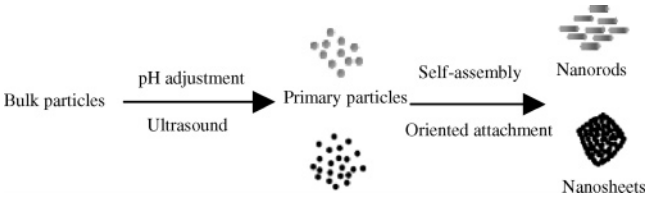

Figure 10. Schematic illustration of the formation of $BiPO_4$ nanorods and BiOCl nanosheets under ultrasonic treatment.

formation of regular nanorods with higher aspect ratios. The nanorods with different aspect ratios were formed during different sonication times, which provides a facile method to control the dimensions of $BiPO_4$ nanorods simply by controlling the sonication time. The growth of BiOCl also showed a similar self-assembly process from primary nanoparticles to lamellar structure under sonication (Figure 9). The coarse fringes of the nanosheets became smooth, indicating the oriented aggregation of nanoparticles at the fringe of the nanosheets and a further crystallization process (Figure 9b, c, and d). A schematic illustration of the sonochemical formation mechanism is shown in Figure 10.

We have also carried out experiments by prolonging the sonication time. It was observed that the dimensions of $BiPO_4$ nanorods increased gradually with the increase in sonication time and the morphology became less uniform, as can be seen in Figure 7f. However, in the case of BiOCl, with the increase in the sonication time, the initial square lamellae fell to irregular small pieces (Figure 9f). The decrease in size may be related to surface corrosion and fragmentation of solids in the presence of high-intensity ultrasonic irradiation. For brittle materials, especially layered inorganic sulfides and oxides, interparticle collisions can induce fragmentation.[38] Therefore, we can see that the interparticle collisions resulting from the ultrasonic irradiation are responsible for both the crystal growth and corrosion/fragmentation of the crystalline solids.

Conclusion

In summary, $BiPO_4$ nanorods with alternative aspect ratios have been successfully prepared, for the first time, via a sonochemical method. Simply by controlling the pH regulator, we can selectively synthesize BiOCl lamellae in the same reaction system, which has been proven to be a new, convenient, and efficient route. The pH value and ultrasonic irradiation played key roles in the formation of 1D and 2D nanostructures. TEM data from samples made after different reaction times suggest an ultrasound-induced nucleation and an oriented-attachment growth mechanism.

Acknowledgment. This work is supported by the National Natural Science Foundation of China (Grant No. 20325516 and 90206037) and the Jiangsu Foundation of China (BK2004210).

IC050674G